25th ABCM International Congress of Mechanical Engineering
October 20-25, 2019, Uberlândia, MG, Brazil

COB-2019-2384
FLOW VISUALIZATION IN AIRFOIL WITH LEADING EDGE PROTUBERANCES APPLIED TO AERODYNAMICS

Fabio Henrique de Paula Bocalon
Letícia Colombari Amadeu
Pedro Vinícius Souza Coimbra
Aluisio Viais Pantaleão
São Paulo State University (Unesp), School of Engineering, Ilha Solteira.
fhpbocalon@gmail.com, colombari.leticia@ieee.org, pedrovinicius19146@hotmail.com and aluisio.pantaleao@unesp.br

Abstract. *One of the main applications of hydrodynamic tunnels, which have been used in several engineering fields since the end of the 19th century, is the understanding of phenomena linked to vehicular hydrodynamics and aerodynamics. Using a vertical hydrodynamic tunnel facility available at UNESP Flow Visualization Laboratory of Ilha Solteira, and continuing with the research previously performed with this apparatus, an experimental work , through flow visualization techniques, was devised with the purpose of understanding and investigating the hydrodynamics of humpback whales, which may result in some performance improvement of airfoils. For this study, two different types of leading edge protuberances on a NACA 63_4-021 baseline airfoil were modeled using 3D prototyping. Changes in the detachment layer position with angle of attack, type of protuberance and chord-based Reynolds number were recorded, inferring some conclusions about drag and lift force in the studied airfoils.*

Keywords: *Hydrodynamic tunnels, 3D Prototyping, humpback whales, hydrodynamics and aerodynamics*

1. INTRODUCTION

Humpback whales are among the largest animals in the world and exhibit the longest flippers of any cetacean, which length varies from 0.25 to 0.33 of total body length (15-16 meters in adult female wales), Tomilin (1957), apud Fish and Battle (1995). Despite their size, these animals have excellent hydrodynamic performance and are capable to produce seemingly impossible water maneuvers, such as large jumps out of the water, Fish and Battle (1995). Another characteristic feature that are related to the performance of this whales are the rounded protuberance tubercles stamped on the leading edge of their fins, which alter the flowfield around them, allowing the flow to remain attached under larger angles of attack.

Fish and Battle (1995) characterized the humpback whale flipper, highlighting its geometric parameters and determining its hydrodynamic performance. In their work, the authors adjusted some NACA 63_4 series airfoils, choosing the NACA 63_4-021 airfoil as the baseline, since its profile resembles a cross section of the humpback whale's flipper. With the knowledge of their results, Johari *et al.* (2007) performed experimental tests in a hydrodynamic tunnel, considering also the same baseline and six other airfoils derived from it, but with different protuberance shapes stamped on the leading edge, baseline and two modified airfoils as shown in the Fig. 1. In the work in focus, aerodynamic coefficients were obtained, such as drag, momentum and lift, as well as images from the flow visualization, useful for analysis of the flow topology around the airfoils studied. Further, according to Johari *et al.* (2007) performance enhancement using such airfoils with leading edge protuberances were noticed.

Paula *et al.* (2016) studied in wind tunnels the airfoils of the series NACA 0012 and NACA 0020, and four other leading edge protuberances, for Reynolds numbers between 50,000 and 290,000, to mimic the humpback whale flippers and evaluate possible aerodynamic enhancements. Other authors such as Hansen *et al.* (2009) and Chen *et al.* (2012)), also described experiments using airfoils similar to that found on humpback whale flippers, all analyzing Reynolds number in the order by Paula *et al.* (2016).

To investigate the effects of Reynolds number on the flow mechanism induced by tubercled airfoils, Rostamzadeh *et al.* (2017) carried out a numerical study. The authors' simulations showed that in contrast to the transitional flow regime in which the unmodified NACA-0021 undergoes a sudden loss of lift, in the turbulent regime the baseline foil experiences gradual stall and produces more lift than the tubercled foil. Their topology analyses revealed some interesting features, such as the cyclic variation in pressure gradient induced by the leading edge tubercles resulting in a higher suction peak to occur in the trough spanwise location. The pressure difference between the trough and the peak drives the flow to

Figure 1. *baseline* (B) , 4S and 4M airfoils respectively . Available From: (Johari *et al.*, 2007)

move towards the trough. On the other hand, the abrupt change in the flow direction in this region leads to strong velocity gradients that account for the turning of the already-present spanwise vorticity within the boundary layer towards the streamwise and transverse directions. Rostamzadeh *et al.* (2017) associated this mechanism to Prandtl's secondary flow of the first type.

Pérez-Torró and Kim (2017) used a Reynolds number of $Re = 1.2 \times 10^5$ and angle of attack $\alpha = 20^{\text{o}}$. They confirmed an increase in lift and reduction in drag and also attributed this benefits to three major events: (i) the appearance of large low-pressure zone near the leading edge created by the laminar separation bubbles (LSBs); (ii) the reattachment of flow behind the LSBs resulting in a decreased volume of the rear wake; and, (iii) the deterioration of von-Kármán (periodic) vortex shedding due to the breakdown of spanwise coherent structures.

Hansen *et al.* (2016) combined experimental and numerical studies and have identified the salient features of the flow structure produced by a NACA 0021 foil with tubercles at Reynolds number of 2230. They have shown that the tubercles lead to an increased flow velocity along the trough, and a larger adverse pressure gradient. The findings of those authors are consistent with a previous research by van Nierop *et al.* (2008), in which they attributed the larger adverse pressure gradient in the trough region to the shorter chord length at this spanwise location. The latter authors also explain that the same pressure difference needed to be overcome over a shorter distance behind a tubercle trough relative to a tubercle peak. They developed a mathematical model for the mechanisms that provide the enhanced characteristics of the wavy airfoils, in opposition to previous researchers, they did not believe that the tubercles might act as vortex generator device because both the wavelength and amplitude of the protuberances were much larger than the boundary layer thickness. Instead, they proposed that the tubercles altered the pressure distribution on the wing such that the separation of the boundary layer was delayed behind the peaks and this phenomena lead to a gradual onset of stall and larger stall angle.

In contrast with van Nierop *et al.* (2008), Wei *et al.* (2015) insisted on that the protuberances worked as vortex generator. Wei *et al.* (2015) carried out an experimental study at a Reynolds of 1.4×10^4, using particle image velocimetry measurements and particle-streak to show that hydrofoils with larger wave amplitudes and smaller wavelengths tended to perform significantly better in flow separation control.

Therefore, the aim of the present work was to investigate the changes in the separation point position considering the troughs and peaks caused by the pressure gradient observed by Hansen *et al.* (2016). The airfoils used were those reported by Johari *et al.* (2007) both the baseline and the ones with protuberances in Fig. 1. Flow visualization techniques were used to characterize the topology of the flow around the foils, with the distinct feature that the tests were carried out exploring Reynolds numbers around 1000 to 1900.

2. MATERIALS AND METHODS

2.1 Experimental facility

The hydrodynamic tunnels are easy to operate and have the advantage of using liquid (water) as a working tool, so it is possible to clearly observe the phenomena that occur in the flow, such as vortices, streamlines, wakes and recirculations once proper dyes are added to the water through small injection needles, in the same flow rate as the tunnel operates.

Uniform flows with low intensity turbulence and small Reynolds numbers are not obtained in the vast majority of aerodynamic tunnels, thus, the use of a hydrodynamic tunnel is a determining factor, allowing for the obtaining of great quality images with better details of the phenomena involved in the flow.

In Fig. 2, there is the schematic of the vertical hydrodynamic tunnel used in the experiments. From this point, the various parts are explained in the sequence.

The tunnel consists of an upper reservoir (RS), equipped with screens and honeycomb (TC), followed by a contraction (CT) where the water is stored for the test rounds, and a test section (ST). To control the flow of water in the tunnel, inside the test section, there is a ball valve (V1), which is able to release water and promote flow. To fill the tunnel, a centrifugal pump is used to draw water from the lower reservoir (RI) through a pipe passing through a butterfly valve (V2), which controls the filling flow of the upper reservoir. Above the top reservoir, there is a discharge diffuser, along with an exhaust outlet, causing the water to drain out of the upper reservoir (RS) when the tunnel is completely full.

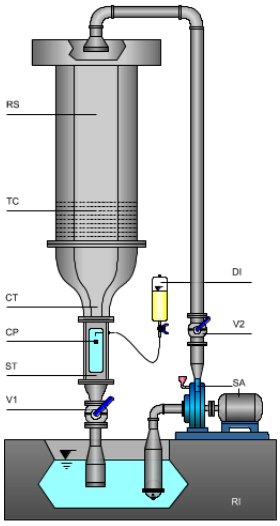

Figure 2. Vertical Hydrodynamic Tunnel Scheme. Available From: Bassan (2011)

The test section of the tunnel, is the location where the airfoil (CP) to be studied is fixed. This section is square with dimensions of 146 x 146 mm with the ends trimmed, being 500 mm long. The matrix that composes the section is made of aluminum and has four acrylic windows, which enable the airfoil to be fixed and the crimping of the dye needles.

Outside the tunnel, just above the test area, two bottles made of PET material and schrader valves are attached. In them the pressurized dye is stored and added to the flow. These bottles are connected to the fine needles by hoses that have their flows controlled by globe valves.

In the present work, a Nikon D90 camera on a tripod was used to take pictures, which, once fixed before the first test, had its position marked so that all the photos were taken from the same point. As for the lens, they had all its parameters analyzed in previous trials and only one setting chosen to be employed throughout the experiment.

2.2 Flow Visualization

In order to visualize the phenomena of the flow around the airfoils, dyes were used, aqueous pigment solution for water-based paint, as adopted in Lindquist. *et al.* (2010), which has great dyeability and low cost. In the vessel pressurizing process, a hose, connected to a compressor, was attached to the valve until a suitable pressure was reached for the experiment, enforcing the same speed as the fluid. The control of the dye flow was purely mechanical, through the opening of an globe valve. Thus, with the continuous flow of water through the tunnel, the injected dyes were forced to follow the water's flow and thereby allowing the fluid stream lines visualization. As the dye was injected at the airfoil's point of stagnation, it was possible to analyze the entire flow around the airfoil, and from these qualitative data, a comparison among the airfoils' lifts.

After being captured, the images were handled with the *ImageMagick* software and the detachment positions were evaluated with the *Inkscape* open source software.

2.3 The Airfoils

The airfoils NACA 63_4-021 used in this work, derived from the study of Johari *et al.* (2007), were built through a 3D printer Makerbot Replicator 2x using PLA filament. However, since the printed airfoils had unwanted roughness due to the printer material deposition method, it was necessary to perform a surface finishing process. In this way, each airfoil was sanded with 300 and 400 sandpaper. After the sanding process, the airfoils were smooth enough for the coefficient of surface friction to be considered the same as for aircraft in the industry nowadays.

The 4S and 4M airfoils are derived from the NACA 634-021 baseline airfoil adding the protuberances at the leading edge. This procedure was made so that the start of its generating function coincided with the edge of the base airfoil, thereby the Mean Aerodynamic Chord of the protruding airfoils matches the baseline aerodynamic winding as well.

2.4 Procedure

The study was divided into three tests for each airfoil, such that nine assays were carried out. Each round was performed by setting a fixed angle of attack and thus by running the test by varying the flow rate, with the Reynolds number range being evaluated from 1000 to 1900.

In each round, the baseline airfoil had nine photos selected for analysis. Meanwhile the airfoils 4S an 4M had eighteen

photos selected each, as the Reynolds number and angle of attack pairs provided information about the flow when the stagnation point was assumed either in the peak or the trough of the protuberance. The Fig. 3 shows the test configuration.

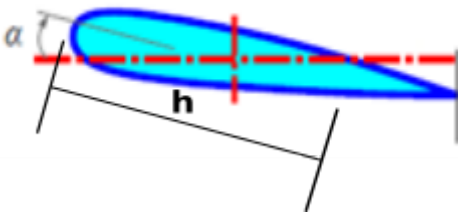

Figure 3. Test Configuration Scheme. From: Own Author

The α angle of attack chosen for the tests were 2°, 6° and 8° for each airfoil. The distance h refers to the measurement of the flow's detachment point at the trailing edge, in millimeters. The assays were carried out similarly to those described in Bocalon *et al.* (2018), and once the angle of attack was set and the tunnel filled with water, the test was accomplished by varying the Reynolds number, which is calculated by Eq. 1.

$$R_e = \frac{\rho V L}{\mu} \tag{1}$$

with:

- ρ as the specific mass of the fluid;
- V as the free flow velocity;
- L as the characteristic dimension, wich was used the mean aerodynamic chord of airfoils;
- μ the absolute viscosity of the working fluid.

For the evaluations of the parameters ρ and μ, the temperature of the water from the tunnel was collected with the aid of a digital thermometer, and the parameters were obtained from Van Wylen and Sonntag (1985) tables.

The filtered images and the measurement of the detachment of the flow to the trailing edge were post processed through the *InkScape* open source software.

3. RESULTS AND CONCLUSION

Once the images were obtained and treated for comparison, five best scenarios were chosen to be analyzed, according to which images were sharper and in what scenario it was possible to better understand the effects of the protuberances on the airfoils aerodynamics. The chosen scenarios, identified by the angle of attack and Reynolds number pairs, were: (2°; 1900), (6°;1000), (6°;1400), (8°; 1400) and (8°; 1900).

According to Johari *et al.* (2007), for the same angle of attack of 6°, the lift coefficient was larger in the 4S foil, with an approximate value of 0.6, while the baseline foil had a lift coefficient close 0.58 and the 4M foil a slightly smaller, but numerically negligible, lift when compared to the baseline. This phenomenon was observed again for the angle of attack of 8°, when the lift coefficient had an approximate value of 0.7 for the 4M foil, an value of 0.8 for the 4S foil and a slightly small value of approximate 0.78 for the baseline foil.

In the same study, Johari *et al.* (2007) concluded that for an angle of attack of 2° the lift coefficient did not have a significant variation, as the coefficient for 4M foil was the same as in the baseline.In his studies, the authors also noted that the variations in drag coefficient between the three profiles for angle 2° and 6° could be neglected, started to differentiate at the angle of 8° with an amplitude of approximately 0.02.

In the present work, the photographic data were used to study the same phenomena described in Johari *et al.* (2007). The results thereafter were obtained from the tests carried out in the UNESP laboratory. As mentioned in the section 2. the distance h was measured on each images and the data are shown in the Tab. 1 in percentage of the aerodynamic chord from the point of stagnation.

Table 1. Distance of the detachment point (h) from the stagnation point in percentage of aerodynamic chord.

α	Reynolds	Baseline (%)	$4S_{peak}$ (%)	$4S_{trough}$ (%)	$4M_{peak}$ (%)	$4M_{trough}$ (%)
2	1900	68.0	72.0	73.0	77.0	67.0
6	1000	58.0	86.9	70.0	78.9	57.0
6	1400	49.0	77.2	63.0	78.4	53.5
8	1400	46.9	78.7	63.7	79.2	54.5
8	1900	67.6	79.4	59.3	72.0	68.4

Source: By the authors.

In the Tab. 1 a clear difference of the detachment point between the peak and the trough is noticed, but in every test the detachment happens further than it does in the baseline airfoil, except for the final scenario.

In Fig. 4, the angle of attack observed (α) is 2°, when the Reynolds parameter was 1900, as shown in Tab. 1 the detachment point in peak and trough of the protuberances can be significantly different, but the average of each foil (4S and 4M) is very close to the baseline.

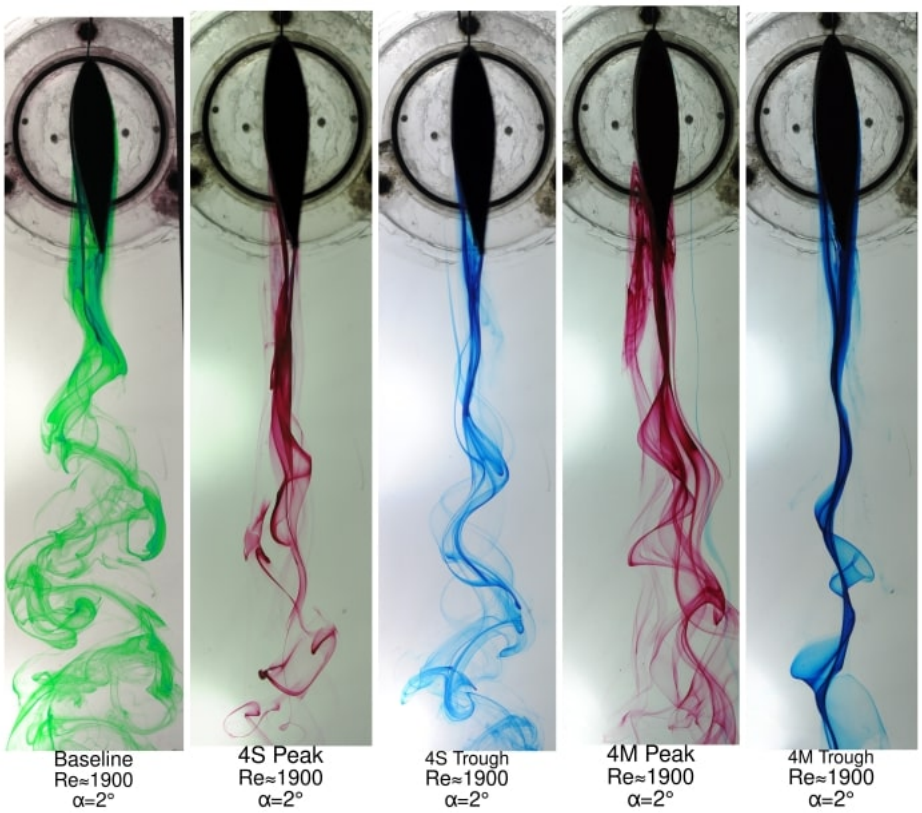

Figure 4. Profile 63_4-021 (baseline), 4S (peak and trough) and 4M (peak and trough), 2°, at Reynolds number 1900 respectively. . Developed by the author.

Compared to the angle of attack of 2°, the angle of 6° has a more clear difference of the detachment point between peak and trough. In this angle of attack its also possible to evaluate a better overall performance of the airfoils 4S and 4M, as both of them have the detachment point further away from the stagnation point when compared to the baseline airfoil and the wake produced by these airfoils are smaller than the one produced by the baseline airfoil.

The Figs. 5 and 6 in the sequence show the data for α of 6 °.

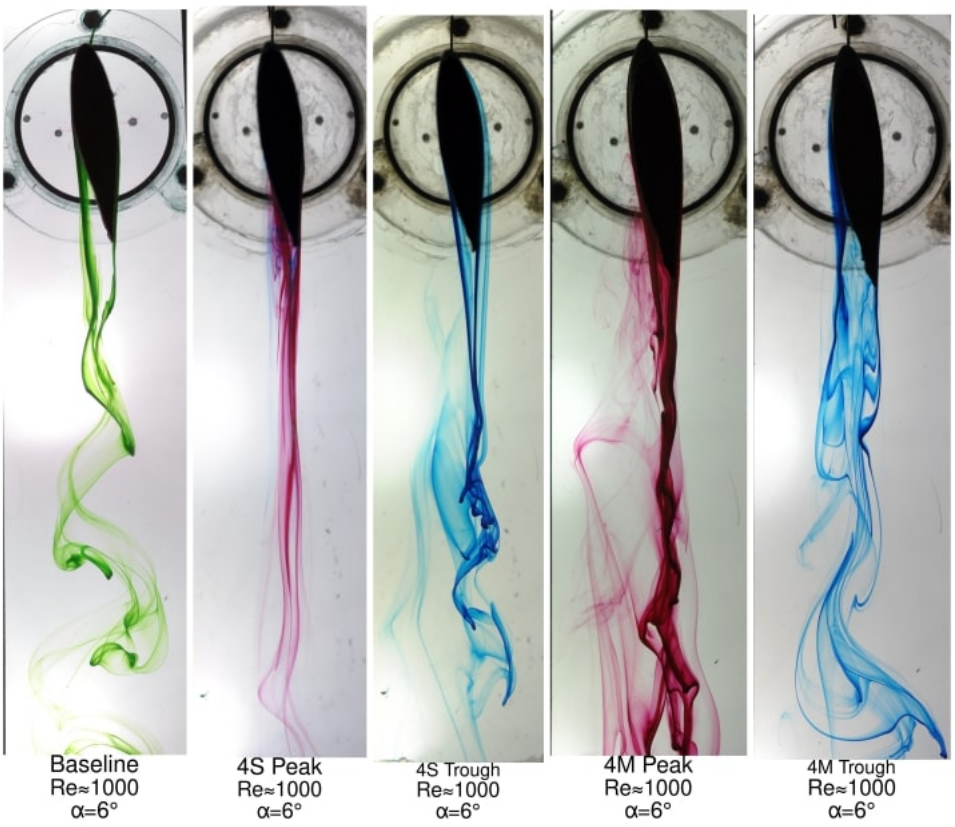

Figure 5. Profile 63_4-021 (baseline), 4S (peak and trough) and 4M (peak and trough), 6°, at Reynolds number 1000 respectively. . Developed by the author.

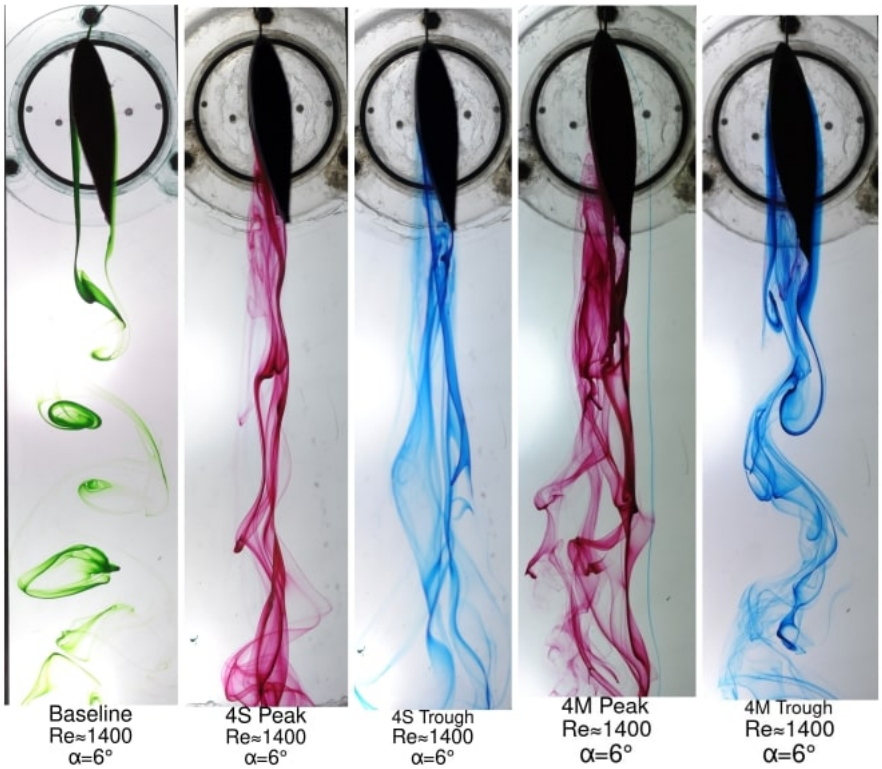

Figure 6. Profile 63_4-021 (baseline), 4S (peak and trough) and 4M (peak and trough), 6°, at Reynolds number 1400 respectively. . Developed by the author.

For the angle of attack of 8° the average detachment point of 4S foil is slightly further when compared to the baseline

foil, and the 4M has the detachment point happens closer to the stagnation point when compared to the 4S foil, although the detachment point is still further from the stagnation point in comparison to the baseline foil. This can be observed in Figs. 7 and 8.

Figure 7. Profile 63_4-021 (baseline), 4S (peak and trough) and 4M (peak and trough), 8°, at Reynolds number 1400 respectively. . Developed by the author.

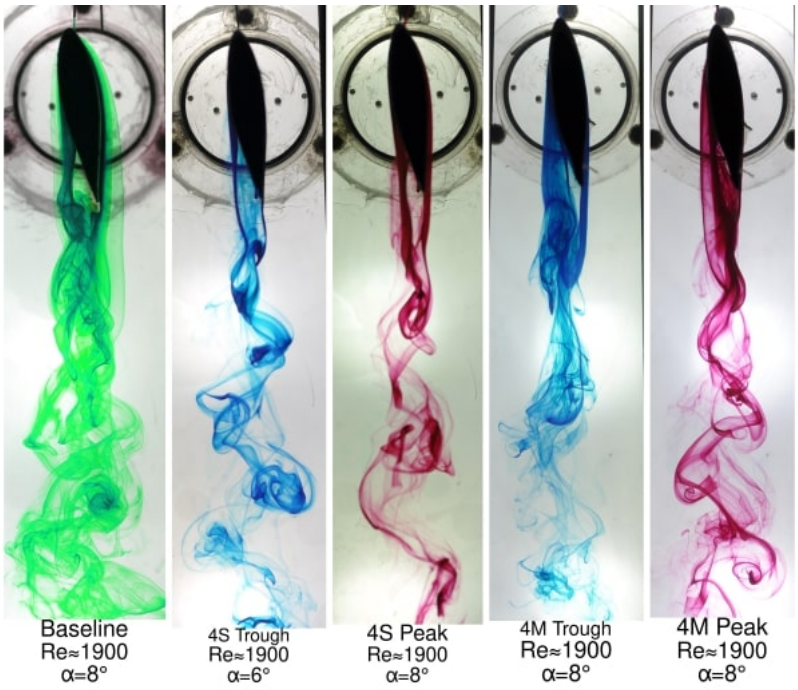

Figure 8. Profile 63_4-021 (baseline), 4S (peak and trough) and 4M (peak and trough), 8°, at Reynolds number 1900 respectively. . Developed by the author.

Given the relationship between the detachment of the boundary layer and the lift coefficient presented in Johari *et al.* (2007), it is possible to conclude that the 4S profile is the one with the highest lift coefficient, corroborating the phenomenon observed by Johari *et al.* (2007).

Although for Reynolds numbers smaller than 1900 von Kármán vortex were observed in this profiles with leading-edge protuberances, indicating energy dissipation (drag), the wake produced by these profiles was very similar to the one produced by the baseline foil. Thus, was inferred that the drag values for these foils should be close for the α studied.

As for the best foil to apply in an aerodynamic design, it can be stated that for the alpha angles studied, the drag coefficient of the baseline foil is minimally smaller than the foils with protuberances due to similarity in the intensity of the vortex shedding (see Fig. 4). This effect was observed by Johari *et al.* (2007) for another range of Reynolds number (Re ≈ 1.83x10^5). This difference in the drag values was negligible when compared to the gain of lift promoted by the protuberances of type 4S with this angle of attack and in the range of Reynolds number studied.

4. ACKNOWLEDGEMENTS

This work has been possible in function of the São Paulo Research Foundation (FAPESP) grants, processes 2019/07947-0 (Regular Process) and 2019/01795-3 (Scientific Initiation).

Our appreciation and thank to professor Dr. Emanuel Rocha Woiski for the proofreading.

5. REFERENCES

Bassan, R.A., 2011. *Visualização experimental de escoamentos no interior de canais munidos de protuberâncias parietais*. Master's thesis, FEIS/UNESP - ILHA SOLTEIRA.

Bocalon, F.H.P., Bueno, D.D. and Pantaleão, A.V., 2018. "Visualização do escoamento ao redor de perfis dispostos em tandem em túnel hidrodinâmico vertical". *Congresso Nacional de Estudantes de Engenharia Mecânica*.

Chen, J., Li, S. and Nguyen, V., 2012. "The effect of leading edge protuberances on the performance of small aspect ratio foils". *15th International Symposium on Flow Visualization.*

Fish, F. and Battle, J., 1995. "Hydrodynamic design of the humpback whale flipper". *Journal of Morphology,225, 51- 60*.

Hansen, K., Kelso, R., Dally, B. and Batill, S.M., 2009. "The effect of leading edge tubercle geometry on the performance of different airfoils". *ExHFT-7,Krakow, Poland*.

Hansen, K.L., Rostamzadeh, N., Kelso, R.M. and Dally, B.B., 2016. "Evolution of the streamwise vortices generated between leading edge tubercles". *Journal of Fluid Mechanics*, Vol. 788, pp. 730–766.

Johari, H., Henoch, C. and Levshin, D.C.A., 2007. "Effects of leading-edge protuberances on airfoil performance". *AIAA JOURNAL Vol. 45, No. 11*.

Lindquist., C., Vieira, E.D.R. and Mansur, S.S., 2010. "Flow around square cylinders in several attack angles". *Proceedings of ENCIT 2010*.

Paula, A.A., Padilha, B.R.M., da S. Mattos, B. and Meneghini, J.R., 2016. "The airfoil thickness effect on wavy leading edge performance". *AIAA SciTech San Diego, California, USA 54th AIAA Aerospace Sciences Meeting*.

Pérez-Torró, R. and Kim, J.W., 2017. "A large-eddy simulation on a deep-stalled aerofoil with a wavy leading edge". *Journal of Fluid Mechanics*, Vol. 813, pp. 23–52.

Rostamzadeh, N., Kelso, R.M. and Dally, B., 2017. "A numerical investigation into the effects of reynolds number on the flow mechanism induced by a tubercled leading edge". *Theoretical and Computational Fluid Dynamics*, Vol. 31, No. 1, pp. 1–32.

Tomilin, A.G., 1957. "Mammals of the USSR and adjacent countries". *Vol. Ix: Cetacea. Moscow: Nauk S.S.S.R. (English Translation, 1967, Israel Program for Scientific Translations, Jerusalem)*.

van Nierop, E.A., Alben, S. and Brenner, M.P., 2008. "How bumps on whale flippers delay stall: An aerodynamic model". *Physical Review Letters*, Vol. 100, No. 5.

Van Wylen, G.J. and Sonntag, R.E., 1985. *Fundamentals of classical thermodynamics*. 536 VAN.

Wei, Z., New, T.H. and Cui, Y.D., 2015. "An experimental study on flow separation control of hydrofoils with leading-edge tubercles at low reynolds number". *Ocean Engineering*, Vol. 108, pp. 336–349.

6. RESPONSIBILITY NOTICE

The authors are the only responsible for the printed material included in this paper.